Lithos 318–319 (2018) 376–385

Contents lists available at ScienceDirect

Lithos

journal homepage: www.elsevier.com/locate/lithos

In-situ lithium isotope geochemistry for a veined jadeitite from the New Idria serpentinite body, California: Constraints on slab-derived fluid and fluid-rock interaction

Naoko Takahashi [a,*], Tatsuki Tsujimori [a,b], Qing Chang [c], Jun-Ichi Kimura [c]

[a] Department of Earth Science, Graduate School of Science, Tohoku University, Aoba, Sendai 980-8578, Japan
[b] Center for Northeast Asian Studies, Tohoku University, Aoba, Sendai 980-8576, Japan
[c] Department of Solid Earth Geochemistry, Japan Agency for Marine-Earth Science and Technology (JAMSTEC), Yokosuka 237-0061, Japan

ARTICLE INFO

Article history:
Received 2 April 2018
15 July 2018
Accepted 7 August 2018
Available online 17 August 2018

Keywords:
Lithium isotopes
Subduction zone
Slab-derived fluid
Fluid-rock interaction
Jadeitite
New Idria

ABSTRACT

Lithium behavior in slab-derived fluids has been constrained using isotope geochemistry of subduction-related metamorphic and volcanic rocks. We investigated a veined jadeitite from the New Idria serpentinite diapir, California, which is regarded as direct precipitates from slab-derived fluids and therefore records slab-derived fluid signatures. We applied an *in-situ* measurement of Li concentration and δ^7Li composition using an ablation volume correction (AVC) LA-MC-ICPMS. This method enabled determinations of millimeter- to submillimeter-scale isotopic variations in the jadeitite veins and host rocks (jadeite matrix), allowing immediate observations on fluid–rock interactions. Multiple-stage jadeite veins and their host rocks showed a wide range of Li concentrations from 4 to 68 μg/g and δ^7Li compositions from −11.7 to +6.7‰, with a curvilinear correlation between them. Individual veins formed in different generations also showed wide isotopic variations as large as ~14‰. Those isotopic and compositional variations within/among veins can be readily explained by variable mixing between the matrix and infiltrated fluids. The initial infiltrated fluid compositions were estimated to be between +6.7 and +12.3‰, based on the δ^7Li values of jadeites in the veins that were supposed to be unmodified by interactions with their matrices. The estimated fluid composition is mostly consistent with those inferred for slab-derived fluids proposed by previous studies. The New Idria jadeitite provides a line of evidence for the presence of high δ^7Li fluids in the mantle wedge at the forearc depth. Our study also demonstrates that the high δ^7Li composition of slab-derived fluids can be easily modified by interactions with surrounding rocks along their pathways.

1. Introduction

Understanding slab-derived fluids is potentially important to solve chemical differentiation in the Earth's interior and the accompanying geologic process, because slab-derived fluids with chemical and isotopic variability affect the compositions of arc lavas, mantle wedge peridotites, and metamorphic rocks in the slab–mantle interface (e.g., Tatsumi and Eggins, 1995). In order to decode the fingerprints of slab-derived fluids in natural rocks and to understand fluid-mediated processes, various geochemical tracers have been used.

In the last two decades, lithium isotope geochemistry has been considered to be a good tracer for mantle-crust recycling, fluid-rock interaction, and fluid mixing and as a geospeedometer (e.g., Halama et al., 2011; John et al., 2012; Marschall et al., 2007; Millot et al., 2010; Penniston-Dorland et al., 2010, 2012; Simons et al., 2010; Taetz et al., 2018; Yang et al., 2015; Zack et al., 2003), due to its mobility in fluids (Brenan et al., 1998) and high isotope fractionation by differences in bond energies between solid and fluid (e.g., Wunder et al., 2006, 2007) and in diffusivities for the two isotopes (^{6}Li and ^{7}Li) (e.g., Richter et al., 1999, 2003). However, the slab-derived Li signature and its contributions to arc magmas remain a matter of debate. Zack et al. (2003) first found very light Li isotopic ratios (hereafter denoted as $\delta^7Li = [(^7Li/^6Li)_{sample}/(^7Li/^6Li)_{SRM8545}-1] \times 1000$) in eclogites from the central Alps; they proposed the Rayleigh dehydration model of subducting slab which postulates that a continuous dehydration caused lighter values in dehydrated rocks and hence progressively slab-derived fluids in ascending order of reaction depth. However, experimental studies (Wunder et al., 2006, 2007) and metamorphic rock data from various localities brought new insights; dehydration of slab materials can cause Li isotopic fractionation between subducting slab and dehydration fluids of only <3‰ (Marschall et al., 2007). Therefore, slab-derived fluids might retain a high δ^7Li signature inherited from a pre-subducted slab composed of altered mid ocean ridge basalt (MORB) (−2.1 to +20.8‰; Chan et al., 1992; Chan et al., 1992, 2002a; Bouman et al., 2004) and

* Corresponding author at: Department of Earth Science, Graduate School of Science, Tohoku University, Aoba, Sendai 980-8578, Japan.
E-mail address: naoko.takahashi.t1@dc.tohoku.ac.jp (N. Takahashi).

https://doi.org/10.1016/j.lithos.2018.08.015
0024-4937/

sediments (−1.7 to +23.33‰; James and Palmer, 2000; Bouman et al., 2004; Chan et al., 2006). The eclogite blocks in mélange in the Franciscan Complex of California record infiltration of high δ^7Li external fluids forming a retrograde blueschist layer (+2.7 to +4.4‰; Penniston-Dorland et al., 2010). Benton et al. (2004) investigated serpentinite muds from the Mariana forearc and found elevated positive δ^7Li values (+4.3 to +7.5‰). Although these studies suggest that slab-derived fluids have a high δ^7Li composition, most studies have reported that arc basaltic rocks globally have δ^7Li values of +1.1 to +7.6‰, with some up to 11.2‰ (Chan et al., 2002b; Moriguti and Nakamura, 1998; Tomascak et al., 2000, 2002), which are similar to those of unaltered MORB (+1.6 to +5.6‰: Tomascak et al., 2008).

In this study, we chose a veined jadeitite from the New Idria serpentinite body, California to reveal the slab-derived Li signatures, because it is regarded as precipitates of slab-derived fluids and has been considered useful for constraining slab fluid composition as well as fluid-mediated metasomatic processes (e.g., Flores et al., 2013; Harlow et al., 2015; Sorensen et al., 2006; Tsujimori and Harlow, 2017). The advantage of the New Idria jadeitite is that the textures of mineral precipitations from fluids and the chemical compositions of vein-filling jadeites both mostly survive against modifications by later events (Takahashi et al., 2017). A pioneering study by Simons et al. (2010) reported whole rock δ^7Li compositions of jadeitites from some global localities; they showed δ^7Li compositions ranging from −1.16 to +2.46‰ and suggested that the jadeitite-forming fluids were mixtures of fluids from bulk altered oceanic crust (AOC) and sediment. However, jadeitite-formations are characterized by multiple stages of fluid infiltration and precipitation including later re-crystallization and re-precipitation (e.g., Sorensen et al., 2006; Tsujimori and Harlow, 2012). Therefore, whole rock δ^7Li composition of jadeitites does not have enough resolution deciphering the fluid-records in the rocks. To avoid complexities from secondary whole rock modification (metasomatic gains and losses of fluid-mobile elements during exhumation) and to take advantage of fossilized multiple-stage fluid-infiltrations with crystal precipitations, we applied an *in-situ* Li isotope study on the veined New Idria jadeitite using a laser ablation-multiple collector-inductively coupled plasma mass spectrometry (LA-MC-ICPMS) technique newly developed by Kimura et al. (2016).

In this paper, we mainly report results of *in-situ* Li isotopic analyses for New Idria jadeitite. We also report trace element concentrations of the jadeitite with various occurrences using a LA-ICPMS. Based on the petrological and CL microscopic study (Takahashi et al., 2017) and new Li isotopic and trace element data of the jadeitite, we characterize behaviors in the slab-derived fluids that formed the multiple-stage veins, and interpret jadeitite-forming fluids at a sub-forearc depth.

2. Geological background and sample description

The investigated jadeitite was collected from the tectonic blocks enclosed within the New Idria serpentinite body (Fig. 1). The New Idria serpentinite body is located in the southern extension of the Diablo Range of the California Coast Ranges between the San Andreas fault on the west and the San Joaquin Valley on the east. The serpentinite body has been considered to be an on-land analogue of active serpentinite diapirs (Atwater et al., 1990; Coleman, 1986; Cowan and Mansfield, 1970; Tsujimori et al., 2007) and to rise from mantle depths, because it encloses blocks of high-grade eclogite which a peak metamorphic condition of T = ~580–620 °C at P > 1.3 GPa (Tsujimori et al., 2007). Although the serpentinite body consists mainly of chrysotile-lizardite serpentinite, the tectonic blocks are surrounded by antigorite serpentinite (Coleman, 1961; Tsujimori et al., 2007).

The investigated jadeitite consists of a pale-greenish and nearly monomineralic jadeitite matrix cut by multiple-stage white jadeite veins (Fig. 2). The matrix is composed mainly of fine-grained impure jadeite with trace amounts of omphacite, Cr-rich omphacite, zircon, allanite and rare titanite; a weak foliation is defined by preferred orientation of the fine-grained jadeite. The matrix has a formation temperature suggested to be <~300 °C because of a wide compositional gap between coexisting jadeite and omphacite. The white veins consist solely of jadeite, which has nearly pure end-member jadeite composition ($NaAlSi_2O_6$). Vein-filling jadeites are characterized by a comb-like structure in which jadeite crystals grow perpendicular to the vein walls, abundant primary fluid inclusions, and oscillatory zoning, which indicate direct precipitation of the crystals from aqueous fluids. Primary fluid inclusions (H_2O and CH_4) are commonly found in vein-filling jadeites. The veins were formed within the jadeite stability condition with a temperature below the brittle–ductile transformation of jadeite. The mineralogy of the investigated jadeitite and associated metamorphic rocks have been described by Coleman (1961), Tsujimori et al. (2007), and Takahashi et al. (2017) in detail. In this study, trace element and Li isotopic compositions of the jadeite were analyzed *in-situ* in both the pale-greenish matrix and the white jadeite veins.

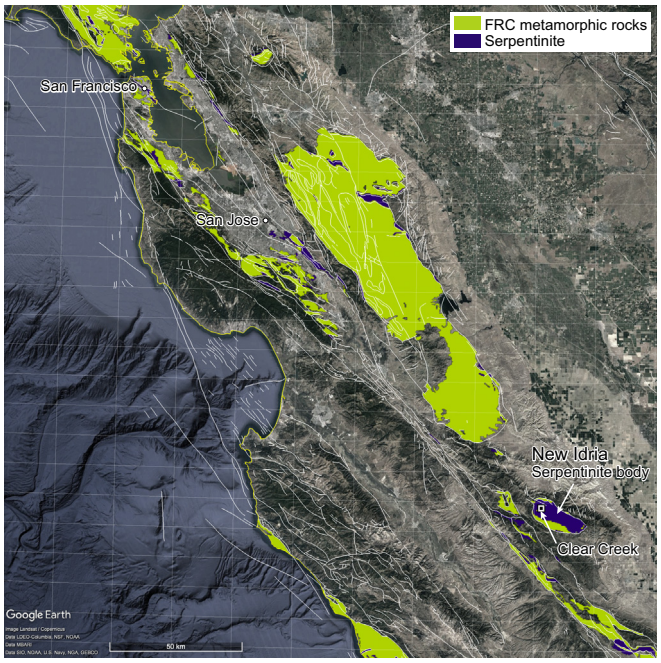

Fig. 1. A map showing sample localities and exposures of the serpentinites and Franciscan (FRC) metamorphic rocks. The base map was created using GoogleEarth and the USGS's California geologic map data (https://mrdata.usgs.gov/geology/state/state.php?state=CA). The investigated jadeitite was collected at Clear Creek in the New Idria serpentinite body.

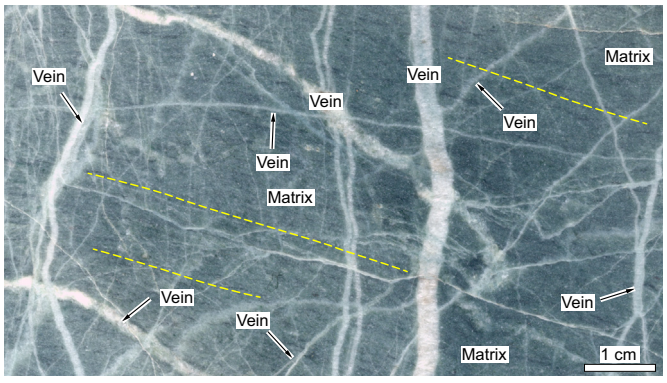

Fig. 2. Scanned image of a polished surface of the investigated jadeitite, showing a cross-cutting relationship between the matrix and veins. The weakly-foliated, pale-greenish jadeite matrix is cut by multiple white jadeite veins of various widths. Yellow dashed lines represent the alignment of foliation.

3. Methods

Thick-sections including multiple generation veins of the New Idria jadeitite were prepared and one side surface polished for *in-situ* trace element and Li isotopic composition analyses. Thin-sections were also made from the opposite surface of the polished thick-sections for observations of the same veins under a petrologic microscope. The polished thick-sections were photographed for CL microscopy, and details of the CL method are referred in Kayama et al. (2011) and Takahashi et al. (2017).

Electron microprobe analyses of the jadeitic clinopyroxenes were carried out with a JEOL JXA-8230 at Okayama University of Science. The analyses were performed with 15 kV accelerating voltage, 12 nA beam current and 3 μm beam size. Natural and synthetic silicates and oxides were used as standards for calibration. The ZAF (oxide basis) method was employed for matrix corrections.

Trace elements (Li, Sc, V, Cr, Co, Ni, Cu, Zn, Ga, Rb, Sr, Y, Zr, Nb, Cs, Ba, La, Ce, Pr, Nd, Sm, Eu, Gd, Tb, Dy, Ho, Er, Tm, Yb, Lu, Hf, Ta, W, Tl, Pb, Th, and U) in the jadeitic clinopyroxenes were simultaneously determined with major elements (SiO_2, TiO_2, Al_2O_3, FeO, MnO, MgO, CaO, Na_2O, K_2O, and P_2O_5) by LA-ICPMS at JAMSTEC; the analysis was performed using an OK Laboratory OK-Fs2000K 266 nm femtosecond laser ablation system with a laser fluence ~12 J/cm^2 at the sample surface at 10 Hz laser pulse repetition rate coupled to a Thermo Fisher Scientific iCAP-Q quadrupole ICPMS. The crater after laser ablation was ~70 μm in diameter and ~30 μm in depth. Standard materials were provided by the United States Geological Survey (USGS), and the BHVO-2G glass used to calibrate all the analyses was made using GSE-1G glass as the standard. Details are referred to Kimura and Chang (2012).

Li isotopic compositions ($^7Li/^6Li$) were determined by LA-MC-ICPMS at JAMSTEC; the analysis was performed using an OK Laboratory OK-EX2000 193 nm nanosecond excimer laser ablation system operated with ~10 mJ/cm^2 laser fluence on the sample surface with laser pulse repetition rate at 10 Hz, coupled to a Thermo Fisher Scientific Neptune multiple Faraday-collector ICPMS. The crater after laser ablation was ~100 μm in diameter and ~45 μm in depth. Calibration was accomplished by bracketing reference materials SRM 612 glass with $^7Li/^6Li = 12.553$ provided by the National Institute of Standards and Technology (NIST). Ablation volume was determined on both the standard glass and the sample jadeite using a digital microscope Keyence VHS-5000. Mass loading dependent $^7Li/^6Li$ isotopic fractionation in the MC-ICPMS and Li concentration in the jadeite samples were corrected for and determined by using the ablation volume correction (AVC) protocol. This method was newly developed by Kimura et al. (2016) and allows simultaneous determinations of Li concentration and δ^7Li from the same laser crater; this study is the first application of their method. Isotopic compositions for Li are normalized to the reference isotope composition $^7Li/^6Li = 12.17$ of NIST SRM 8545 (LSVEC, Li carbonate [Li_2CO_3]) by $\delta^7Li = [(^7Li/^6Li)_{sample}/(^7Li/^6Li)_{SRM8545}-1] \times 1000$. Both the repeatability and the laboratory bias of δ^7Li measurements using the AVC protocol were within ±1‰ (2SD). Details of the method can be found in Kimura et al. (2016).

4. Results

4.1. Microstructures

In the investigated sample, subcentimeter-scale to submillimeter-scale white jadeite veins of multiple generations cut the pale-greenish weakly-foliated matrix (Fig. 2). The cross-cutting relationships of those veins define the relative timing of crack-sealing and jadeite precipitation events. Microstructural analyses show at least four vein phases: v_1, v_2, v_3 and v_4 (Fig. 3). The v_1 is the earliest form of vein, and is cut by v_2, v_3 and v_4. Although the v_4 veins are further divided into v_{4a} and v_{4b}, the cross-cutting relationship is not clear. Vein-widths tend to be narrower for later.

The vein v_1 consists mostly of coarse-grained, euhedral, and fibrous jadeites oriented perpendicular to the vein walls (Fig. 3a, b). The crystal size ranges from small near the vein walls to as big as from one side to the other of the vein. The boundary between the v_1 and the matrix is not clear as some crystals seem to penetrate the matrix. Color CL image shows dark luminescent portions in the v_1 margin. Narrow bands consisting of subhedral to euhedral, Ca, Mg and Fe-rich impure jadeites are found only in the v_1 margin (Fig. 3c). The v_2 crosscutting v_1 also consists mostly of coarse-grained euhedral to subhedral and fibrous to blocky jadeites oriented perpendicular to the vein walls (Fig. 3d, e). Blocky textures are produced by primary crystallization and not re-crystallization; CL images show remarkable oscillatory growth zoning. Color CL image also shows dark luminescence of impure jadeites in the v_2 margin. The v_3 is characterized by coarse-grained, euhedral and fibrous jadeites oriented perpendicular to the vein walls. The latest v_{4a} and v_{4b} are found as small veinlets, and the orientation of the vein-filling jadeites is aligned to a foliation of the pale-greenish matrix (Fig. 3d, f). Compositional differences of major and trace elements for each site are described below.

4.2. Major elements

Representative electron microprobe analyses are given in Table S1 and Takahashi et al. (2017); a compositional traverse on a line perpendicular to a jadeitite vein is shown in Fig. 4. The traverse across the v_1 (Fig. 4) reveal an increase in impurities from the center to the vein walls. The veins consist solely of jadeite with a nearly pure end-member jadeite composition (Jd_{95-100}; 0.01–0.68 wt% CaO, 0–0.56 wt% MgO; 0–1.5 wt% FeO), whereas the matrix has significant impurities with a variable CaO (0.12–5.37 wt%), MgO (0.01–3.69 wt%), and FeO (0.22–4.46 wt%) (Jd_{72-100}). Color CL image shows dark luminescent portions in the v_1 margin (Fig. 3a), which have also impurities of CaO, MgO, and FeO (Jd_{86-97}; 0.39–1.85 wt% CaO, 0.22–0.64 wt% MgO, 0.39–2.42 wt% FeO). Bands consisting of subhedral to euhedral, Ca, Mg, and Fe-rich impure jadeites in the v_1 margin contain 2.63–3.99 wt% CaO, 1.89–2.97 wt% MgO, and 1.30–3.83 wt% FeO (Jd_{74-82}).

We have reported fairly good agreements between EPMA and LA-ICP-MS major element results elsewhere (Kimura and Chang, 2012). For the present dataset, we compared the results of averaged vein and matrix compositions. Analytical biases for major elements (>1 wt%) were shown to be SiO_2 < 0.8%RD (%RD: % relative deviation), Al_2O_3 < 2%RD, FeO < 11%RD, MgO < 8%RD, CaO < 6%RD, and Na_2O < 1.5%RD, with overall correlation of element abundances given by $Y_{LA\text{-}ICPMS} = 0.9936 \times X_{EPMA}$ and a $r^2 = 0.9999$ correlation coefficient.

4.3. Trace elements

The trace element concentrations of 31 analyzed spots at matrix jadeites and vein-filling jadeites (v_1, v_2, v_3, v_{4a} and v_{4b}) in the New Idria jadeitite are shown in Table S2. Spot analyses found several important characteristics: (1) The jadeite we investigated is enriched compared to N-MORB in some large-ion lithophile elements (LILEs) — Li (≤48 μg/g) and Cs (≤8 μg/g)— and some high field strength elements (HFSEs) —Ta (≤3 μg/g), Nb (≤234 μg/g), U (≤3 μg/g), and Th (≤6 μg/g) —. These features can be recognized as prominent spikes in the N-MORB normalized trace elements patterns plotted in Fig. 5. (2) Overall, trace element abundances vary widely within a sample and a vein, in up to two orders of magnitude. Within a sample, later precipitated veins (v_3, v_{4a}, and v_{4b}) show higher abundances of almost all trace elements, excepting HFSEs, than in the earliest precipitated vein (v_1). Within veins, v_1 and v_2 have large variations, although no variation could be found from v_3, v_{4a}, and v_{4b} due to a limited number of LA-ICPMS analyses. (3) In the v_1, the vein margin has high abundances of almost all trace elements except HFSEs and no strongly positive Eu anomaly in

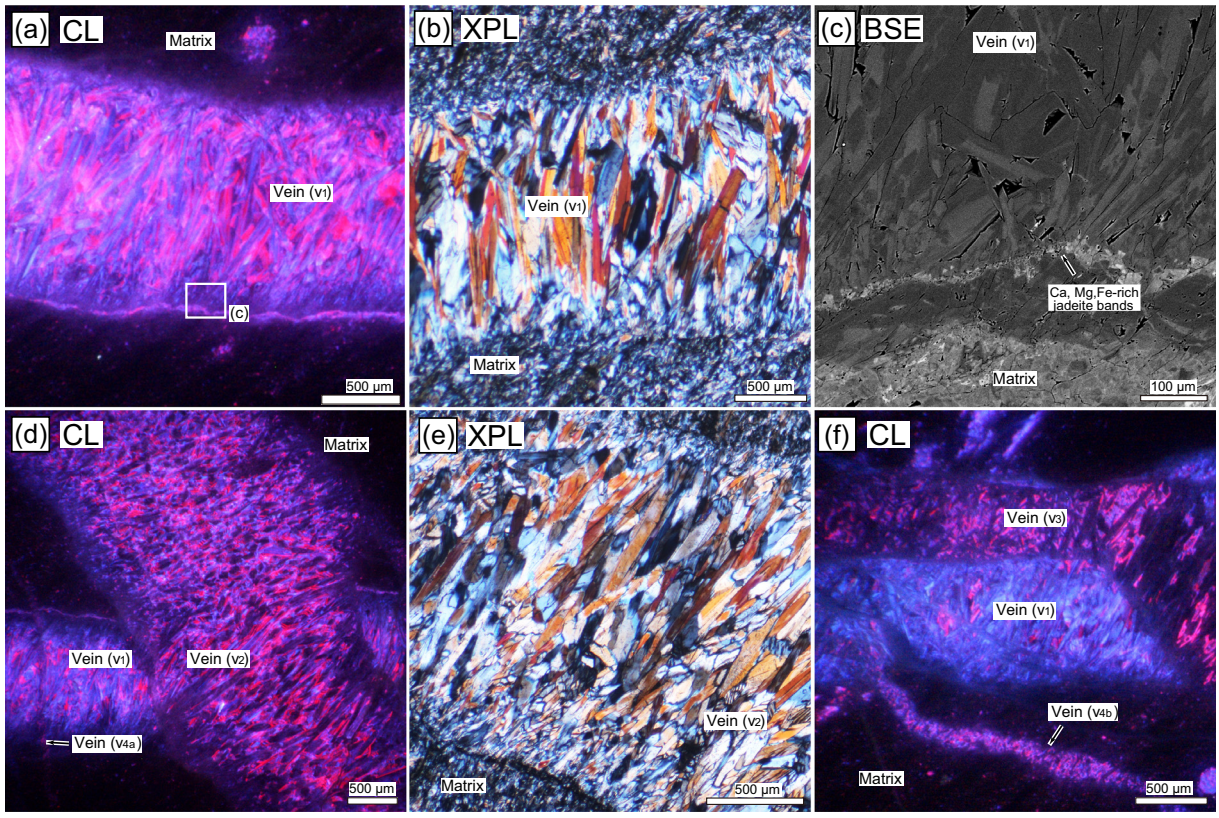

Fig. 3. Microtextures of the investigated jadeitite. The veins (v_1, v_2, v_3, v_{4a} and v_{4b}) are numbered in order of the relative timing of their formation, with v_1 being the earliest formed vein; the relative timing among v_{4a} and v_{4b} is unclear. (a) Optical cathodoluminescence (CL) images of vein v_1 (bright luminescence, red, blue, and dull blue-CL) cutting the pale-greenish matrix with dark luminescence. Note that the vein margin of v_1 also shows dark luminescence. (b) Crossed-polarized (XPL) photomicrograph of the v_1, showing fibrous crystal orientation perpendicular to the vein wall. (c) Back-scattered electron (BSE) image of the boundary between the v_1 and the matrix. Note that Ca, Mg and Fe-rich jadeite bands occur in the v_1 margin. (d) Optical-CL image of the v_2 cutting the v_1. The v_2 margin exhibits dark luminescence. (e) XPL photomicrograph of the v_2, showing fibrous to blocky crystal orientation perpendicular to the vein wall. (f) Optical-CL image of a cross-cutting relationships of several veins.

contrast to the center of the vein. (4) The matrix shows clearly different patterns from vein-filling jadeites; they have higher abundances of almost all trace elements and no strong peaks of Nb and Ta compared to the veins. Although data on matrix jadeites are limited to one spot analysis, the feature of the matrix jadeites is supported by the analysis of the v_1 + matrix boundary (spot tr# 25; see Table S2), which also shows a trace element-rich pattern. (5) The Li versus CaO plot (Fig. 6) suggests that purer, i.e., close to end-member composition jadeites contain more Li than impure jadeites. Moreover, the chemical compositions of vein margins and later precipitated veins are closer to that of the matrix.

4.4. Lithium concentration and isotopic composition

The Li concentration and δ^7Li composition of 40 analyzed spots at matrix and vein-filling jadeites (v_1, v_2, v_3, and v_{4a}) in the New Idria jadeitite are shown in Table 1 and Fig. 8. Our data suggest that: (1) Li concentration and δ^7Li within the jadeites varied widely ranging from 4 to 68 μg/g and from −11.7 to +6.7‰, respectively; these values show distributions along a curvilinear correlation regardless of the vein generation and the occurrence. (2) Li concentration and δ^7Li within an individual vein also vary widely. For example, the v_1 shows Li concentrations ranging from 8 to 68 μg/g and δ^7Li ranging from −6.9 to +6.7‰; the v_1 margin has low Li concentration and δ^7Li relative to the center of the vein. In addition, the v_2 shows Li concentrations ranging from 7 to 19 μg/g and δ^7Li ranging from −11.7 to +1.6‰. The extremely low −11.7% δ^7Li was found near the vein walls, although the other side of the margin which is not in contact with the matrix did not show such low values. (3) Li concentration and δ^7Li among the veins tend to have higher Li concentration and δ^7Li in earlier precipitated veins than in veins precipitated later. This relation is at least shown by the mean values of v_1 (26 μg/g and +1.5‰) and v_2 (11 μg/g and −2.5‰) from >10 spots analyses conducted on them. (4) The matrix shows low Li concentrations ranging from 6 to 13 μg/g (mean: 9 μg/g) and low δ^7Li compositions ranging from −10.8 to −4.4‰ (mean: −8.2‰).

5. Discussion

5.1. Vein formation conditions

Vein microstructures preserve mineral growth conditions during vein formation. The investigated jadeite veins are mostly syntaxial veins where the vein-filling minerals grow from both sides of vein walls towards the center (e.g., Bons et al., 2012). The different growth rates of individual vein-filling jadeites result in growth competition as a characteristics of syntaxial veins (e.g., Okamoto and Sekine, 2011). In general, wall-rock inclusions, secondary minerals, or fluid inclusions are found at the frontal surfaces of the syntaxial vein growth, which reveal crack-sealing events during vein formation (e.g., Ramsay, 1980). As descried above, thin bands consisting of euhedral Ca, Mg and Fe-rich impure jadeites ($Jd_{74–82}$) were observed only in the v_1 and these jadeites have similar composition to those in the matrix. The observed vein microstructures imply that jadeite veins in the New Idria jadeitite formed from single- or two-cracking events which created the space for jadeites to grow into. Moreover, major and trace element analyses revealed that jadeites in the vein margins which have impurities of CaO, MgO and FeO ($Jd_{86–97}$) and trace elements-rich characteristics in contrast to the pure

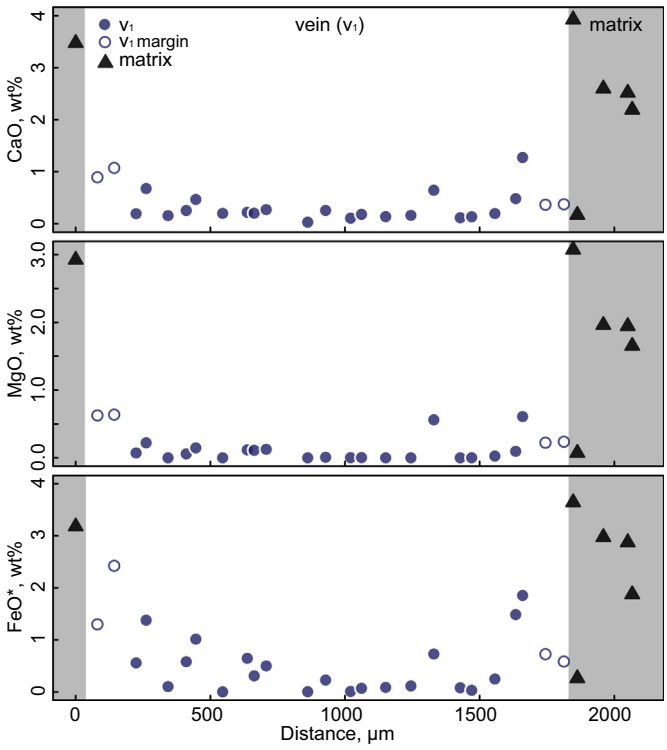

Fig. 4. Compositional traverse across a jadeitite vein (v_1) showing changes of selected impurities (CaO, MgO, and FeO*). The gray field represents the pale-greenish matrix.

jadeites ($Jd_{95–100}$) from vein centers, were affected by the matrix which also contains significant impurities ($Jd_{72–100}$). These results imply dissolution of the matrix jadeite into infiltrating fluids and re-precipitation of impure jadeites with intermediate compositions between the matrix and infiltrating fluids near the vein walls during the earliest stage of vein formation. Subsequent (re-fracturing and) precipitation of newly infiltrating fluids formed pure jadeites in the center of the veins. Narrow veinlets (v_{4a} and v_{4b}) are also supposed to be chemically affected by matrix components.

The observations described above strongly suggest that the chemical compositions derived from a pristine fluid that formed earlier precipitated veins were likely not affected by chemical components derived from the matrix, except for the vein margins which were in contact with the matrix. Moreover, the later precipitated veins, which were more enriched in CaO, MgO, and FeO, are supposed to have experienced greater interactions between infiltrated fluids and the matrix as fluid circulation in the host rock proceeded.

5.2. The source of jadeite-forming fluid

Global jadeitite-forming fluids have multiple sources or evolution steps in their composition along their flow paths, which have suggested by CL-guided trace element and oxygen isotope data (Sorensen et al., 2006). Oxygen isotopes of red and blue-CL domains are different from those of green-CL domains in the Myanmarese jadeitite (Sorensen et al., 2006), which implies that the difference of CL color may reflect multiple sources of jadeitite-forming fluids. The New Idria jadeitite also shows distinct repeated zoning in ~50 μm scales of red-CL and blue-CL domains corresponding to their compositional differences (Takahashi et al., 2017). However, oxygen isotopes of red- and blue-CL domains in the New Idria jadeitite show relatively homogeneous values with a high $\delta^{18}O$ composition (+8.4 to +9.9‰; Sorensen et al., 2006). The difference of CL color in the New Idria jadeitite may thus reflect not multiple sources of fluids, but instead, it would be a self-organization process inherent to the crystallization mechanism without intervention of an external fluids (e.g., Wang and Merino, 1992). The high $\delta^{18}O$ composition also implies that the jadeite-forming fluids were derived from low-temperature altered sediments or oceanic crust. Patterns of N-MORB normalized trace elements (see Fig. 5) show a similarity to that of global subducted sediment composite (GLOSS) from Plank and Langmuir (1998), which has the potential to elevate LILEs, U, Th, Zr, Nb, and Ta (Harlow et al., 2015). Taking this into account, our trace

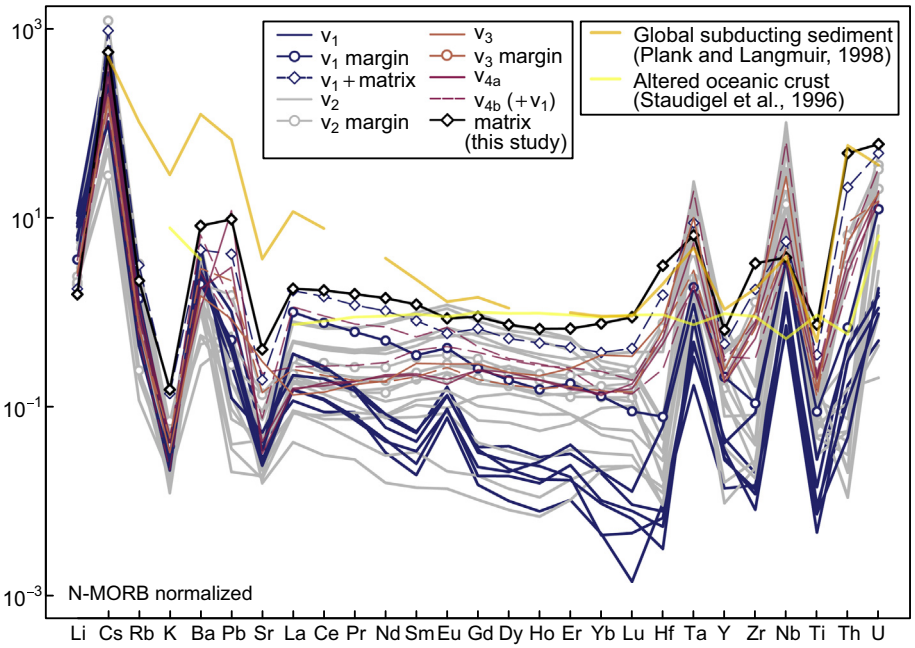

Fig. 5. N-MORB normalized trace element patterns of the New Idria jadeitite. Normalization factor and reference values are from McDonough and Sun (1995), Plank and Langmuir (1998) and Staudigel et al. (1996).

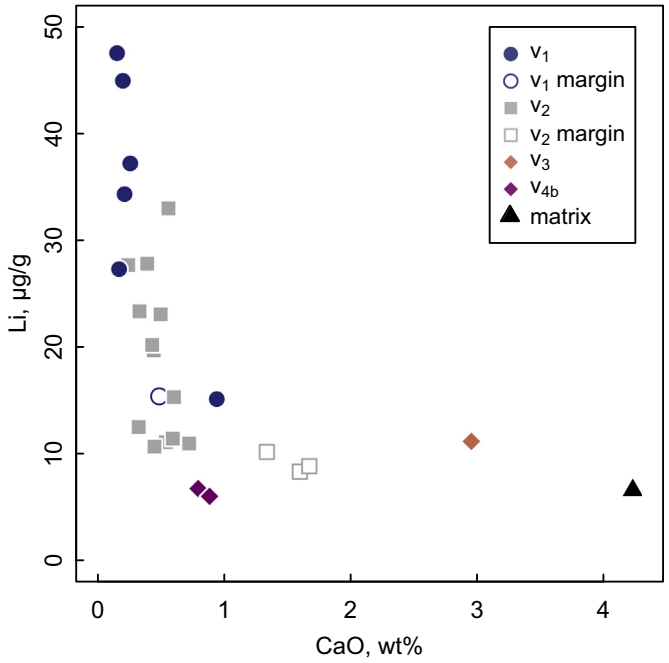

Fig. 6. Li versus CaO diagram showing compositions of jadeites in different occurrences.

element analyses suggest that the New Idria jadeite-forming fluids were derived metasedimentary rocks.

We compare the New Idria vein-filling jadeites with experimentally determined fluid compositions in equilibrium with Plank and Langmuir (1998)'s GLOSS and upper continental crustal materials, i.e., metamorphosed sediments at 2.5 GPa and 600 °C (Hermann and Spandler, 2008) (Fig. 7). Note that the experimental conditions have much higher pressure and temperature than the New Idria jadeitite-forming *P–T* regime; due to the difficulty of performing experiments at low-temperature, such data are extremely limited in the literature. Moreover, Kimura et al. (2014) and Kimura (2017) proposed elemental mass balance in the subducted slab layers, including considerations on prograde metamorphism of the host protoliths and chromatographic reactions of the dehydration fluid in the hosts; low temperature (~2 GPa and 300 °C) slab fluid compositions calculated using the Arc Basalt Simulator ver.5 (ABS5) model for sediment and AOC compositions (Kimura, 2017; Kimura et al., 2014) are also plotted in Fig. 7. Although the degree of equilibration between precipitated jadeites and jadeite-forming fluids could not be quantified, the fluid composition in equilibrium with the vein-filling jadeites can also be calculated using trace element partitioning coefficients between clinopyroxene and aqueous fluid which were determined by piston-cylinder experiments at 1.0 GPa and 950 °C (Adam et al., 2014).

Notwithstanding the assumptions with large uncertainties, the key features of the trace element patterns of experimentally determined fluids in equilibrium with sediments resemble those of the New Idria vein-filling jadeites themselves and the fluid compositions calculated from the vein-filling jadeites, in terms of REEs, U, and Th. Slab fluid composition calculated using the ABS5 model for the sediment is relatively more similar to that of the New Idria jadeitite than AOC composition. In contrast, Nb and Ta showing strong positive spikes in the New Idria vein-filling jadeites and their fluids are exceptions. Possible reasons for high Nb and Ta concentrations in the New Idria jadeitite include: (1) Nb and Ta are highly concentrated in the jadeite-forming fluids due to a lack of rutile in the fluid source, which largely controls the budget of these elements in the oceanic crust (e.g., John et al., 2011). (2) The published mineral–aqueous fluid partitioning coefficient determined by high-temperature experiments cannot be applied to the New Idria jadeitite, which formed at low temperature, because of its high temperature-dependence. (3) Other factors such as crystal-chemical effects (Blundy and Wood, 1994; Marks et al., 2004), which might play a subordinate role in element partitioning.

Table 1
In-situ Li concentration and δ^7Li analysis values of the New Idria jadeitite.

Spot iso#	Remark	Li, μg/g	error (2σ)	δ^7Li, ‰	error (2σ)
Jade-2	v1	10.9	1.1	−3.8	1.7
Jade-3	v1	5.6	3.5	−0.7	1.6
Jade-9	v1	13.8	0.5	−0.6	1.3
Jade-10	v1margin*	10.2	3.5	−4.8	1.9
Jade-11	v1	28.6	5.5	5.8	0.9
Jade-12	v1	68.3	1.1	6.7	0.9
Jade-13	v2margin*	13.5	0.9	−1.8	1.3
Jade-14	v2	15.0	0.3	1.1	1.2
Jade-15	v2	11.7	1.5	−3.0	1.4
Jade-16	v2	18.7	0.8	0.7	1.3
Jade-17	v2	10.4	0.7	−0.4	1.5
Jade-18	v2	14.0	1.4	−2.3	1.2
Jade-19	v2	16.1	0.5	−0.3	1.6
Jade-20	v2	8.2	1.4	−4.3	1.9
Jade-22	v2	7.5	0.5	−2.9	1.9
Jade-23	v2	8.7	0.4	−1.9	2.2
Jade-24	v2	18.8	1.0	1.6	1.1
Jade-25	v2	7.9	0.6	−6.1	2.2
Jade-26	v2	7.0	0.4	−11.7	2.4
Jade-27	v2margin*	6.9	0.3	−4.9	2.0
Jade-30	v2	7.5	0.3	−5.0	2.4
Jade-31	matrix	7.2	0.4	−10.8	2.9
Jade-32	v1margin*	16.8	1.1	−0.2	1.4
Jade-33	v1	32.8	2.4	4.8	1.1
Jade-34	v1	33.1	1.7	3.3	0.8
Jade-35	v1	26.3	2.7	0.0	1.6
Jade-36	v1	23.7	2.0	1.2	1.7
Jade-37	v1	24.9	1.2	5.3	1.0
Jade-38	v1	34.3	1.9	4.9	1.2
Jade-39	v1	38.6	3.2	4.7	1.1
Jade-41	v4a	4.3	0.1	−8.1	3.4
Jade-42	v4a	4.0	0.1	−8.8	4.1
Jade-43	matrix	9.9	0.4	−8.6	1.6
Jade-46	matrix	12.9	0.5	−4.4	1.5
Jade-51	v1	10.9	0.4	−3.2	1.4
Jade-52	v3	11.2	0.4	−5.9	1.4
Jade-53	v3	10.5	0.3	−8.0	1.7
Jade-54	v3	6.5	0.1	−9.5	2.5
Jade-55	v3	11.4	0.3	−1.5	1.7
Jade-57	matrix	6.3	0.2	−8.9	2.7

* Vein margin is defined by the spot within ~100 μm from the boundary between the matrix and the vein.

5.3. Lithium concentration and isotope systematics

In-situ Li concentration and δ^7Li analyses in this study detected the variations in the millimeter- to submillimeter-scales. The New Idria jadeitite shows wide variations of Li concentration and δ^7Li, ranging from 4 to 68 μg/g and from −11.7 to +6.7‰, respectively; these values show distributions along a curvilinear correlation regardless of the vein generation and the occurrence (see Fig. 8a). The - δ^7Li value of −11.7‰ is extremely low in comparison to reported Li isotopic compositions of the metamorphic rocks. To address the processes affecting variations in Li concentration and δ^7Li at short spatial scales, we first discuss the effect of the diffusion process and then consider a possible scenario to produce variations of Li concentration and δ^7Li.

5.3.1. Effect of diffusion process to produce variations

Diffusion is one of the important mechanisms producing the Li isotopic variations because of different diffusivities of ^{6}Li and ^{7}Li. Diffusion is orders of magnitude faster for Li than other elements (e.g., Coogan et al., 2005; Richter et al., 1999, 2003; Teng et al., 2006), therefore large Li isotopic variations can be produced even at low temperatures and within

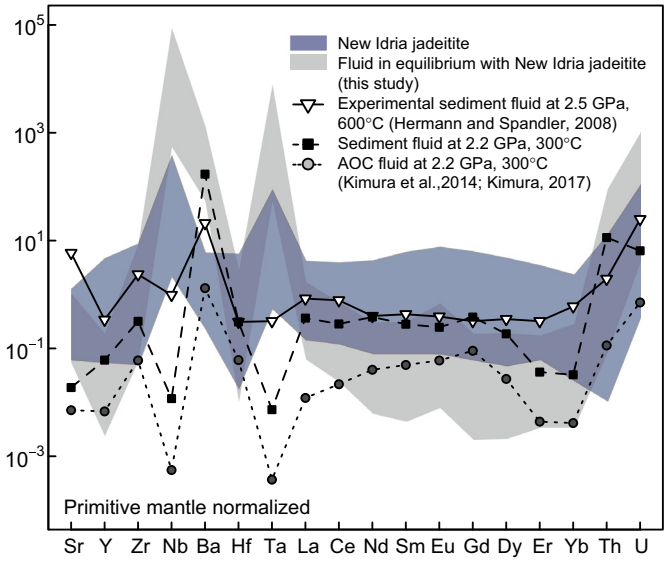

Fig. 7. Primitive mantle-normalized trace element pattern for the New Idria jadeitite (blue domain) and inferred fluid in equilibrium with the vein-filling jadeites (gray domain) using partitioning coefficients (Adam et al., 2014). For comparisons, experimentally determined fluid composition at 2.5 GPa and 600 °C (Hermann and Spandler, 2008) and low temperature (~2 GPa and 300 °C) slab fluid compositions calculated using the Arc Basalt Simulator ver.5 (ABS5) model for the sediment and AOC compositions (Kimura, 2017; Kimura et al., 2014) are also plotted.

relatively short time scales. Our Li isotopic data of the New Idria jadeitite show that the v_1 has the profile of the spots iso# -33, 32, and 31 with decreasing Li concentrations and δ^7Li (Fig. 8b). If we assume that the vein initially had higher Li concentrations, and then the gradients may have been produced by diffusion of Li from the Li-rich vein to the Li-poor matrix in the ascending serpentinite body as well as after vein crystallization. Verifying the effect of diffusion process requires to postulate the temperature values which the New Idria jadeitite had experienced in the serpentinite body after vein crystallization and the temperature-dependent diffusion coefficient for Li in clinopyroxene. The formation temperature of the New Idria jadeitite has not been completely examined in previous studies; however, a wide compositional gap between coexisting jadeite and omphacite of the pale-greenish matrix in the New Idria jadeitite suggests its formation conditions of $T <$ ~300 °C (Tsujimori et al., 2005, 2007). Moreover, jadeite-bearing retrograded eclogite including sodic amphibole, jadeite, lawsonite, and pumpellyite as tectonic blocks in the New Idria serpentinite body, is considered to have formed at the same time as the New Idria veined jadeitite investigated in this study (Tsujimori et al., 2007). The existence of pumpellyite in the retrograded eclogite suggests that it formed in a temperature range for pumpellyite-zone metabasites of $T = 200$–290 °C (Maruyama and Liou, 1988). Therefore, we concluded that the experienced temperature of the investigated New Idria veined jadeitite had been < ~300 °C. The diffusion coefficient for Li in clinopyroxene at 300 °C is 8.9×10^{-26} m^2 s^{-1}, which is taken by extrapolating from diffusion coefficients for Li in diopside determined by experiments at 800–1200 °C (Coogan et al., 2005). If these assumptions hold true, the diffusion coefficient of 8.9×10^{-26} m^2 s^{-1} eliminates diffusion on a several hundred μm-scale over a geological timescale (e.g., a significant diffusion length $\sqrt{Dt} =$ ~1 μm, where diffusion coefficient is 8.9×10^{-26} m^2 s^{-1} and duration time is 10^7 yrs). We could not describe more discussions here because of a lack of data, such as diffusion coefficients at low temperature. However, the traverse of major elements across a vein (Fig. 4) also shows several hundred μm-scale gradients from the center of the vein to the vein walls, despite of smaller diffusion coefficients of Ca, Mg, and Fe than Li. Therefore, this indicates that the diffusion process is unlikely to explain the isotopic variations in the New Idria jadeitite.

5.3.2. Possible scenario to produce the variations of Li concentration and δ^7Li

Vein microstructures and chemical compositions suggested that infiltrated jadeitite-forming fluids were chemically affected by the matrix during vein formation. Moreover, the lowest δ^7Li value in the vein is observed near vein walls, and do not significantly exceed the lowest δ^7Li value in the matrix. Therefore, we conclude that the isotopic variations in the veins can be attributed predominantly to variable mixing of infiltrating fluids and chemical components from the matrix. Considering the likely case that the vein-filling jadeites were not perfectly in equilibrium with fluids because of rapid propagation of the veins, the jadeite fractional crystallization mechanism may also be of importance in Li isotopic fractionation.

In this paper, we postulated a partial dissolution of the matrix that triggered by infiltrating fluids with consequent re-precipitation to form new jadeite crystals with mixing between infiltrating fluids and chemical components from the matrix as the most reasonable scenario. In this scenario, Li concentration and isotopic variations can be modelled as two end-member mixing between the matrix and an infiltrating fluid. We assumed that the precipitated jadeites directly reflected the composition of fluids; note that the degree of equilibration between precipitated jadeites and infiltrating fluids could not be quantified. Using the highest Li concentration and δ^7Li in jadeites of the v_1 (68 μg/g and + 6.7‰) as an end-member *a* and the lowest Li concentration and δ^7Li in the matrix (7.2 μg/g and − 10.8‰) as another end-member *b*, the mixing model fits variations in the observed data (Fig. 8). The mixing equations are expressed as:

$$C = C_a \times f + C_b \times (1-f)$$

and

$$\delta^7\mathrm{Li} = \left(\delta^7\mathrm{Li}\right)_a \times f + \left(\delta^7\mathrm{Li}\right)_b \times (1-f)$$

where C represents Li concentration and *f* represents fraction of Li in end-member *a*.

As shown in Fig. 8a, not only the data of the v_1 but also other data from all veins and the matrix lie on the mixing line, which implies that the variations in the investigated sample might be produced by a common process in all the veins. Thus, the jadeite-forming fluids in all veins would be from a single source. We assume that the highest Li concentration and δ^7Li in jadeites of the v_1 (68 μg/g and +6.7‰) as an end-member *a* represent a more likely initial infiltrating fluid composition, because its value is in the center of the earliest precipitated vein, which was not likely affected by chemical components derived from the matrix. In essence, the variations in the investigated jadeitite can be interpreted as resulting from various degrees of interaction between a single source fluid and the host rock in various fluid pathways in the jadeitite body.

5.4. Implication for geochemical characteristics of subduction zone fluids at sub-forearc depth

In the investigated jadeitite, the highest Li concentration and δ^7Li (68 μg/g and +6.7‰) in the center of the earliest precipitated vein (v_1) would represent a fossilized composition of initial infiltrating fluids. Although our assumption is that vein-filling jadeites were not in equilibrium with the jadeite-forming fluids due to fast vein formation, we solved the maximum δ^7Li value of the initial infiltrating fluids that formed the jadeites with the highest Li concentration and δ^7Li (68 μg/g and +6.7‰) by assuming fluid precipitation under perfect equilibrium conditions. The calculation used the fractionation factor at 300 °C from Wunder et al. (2006) at which temperature corresponds with the formation condition of the matrix as the host rock, and resulted in a maximum δ^7Li fluid composition of +12.3‰. For instance, the initial slab-derived fluids that formed the New Idria jadeitite are supposed to

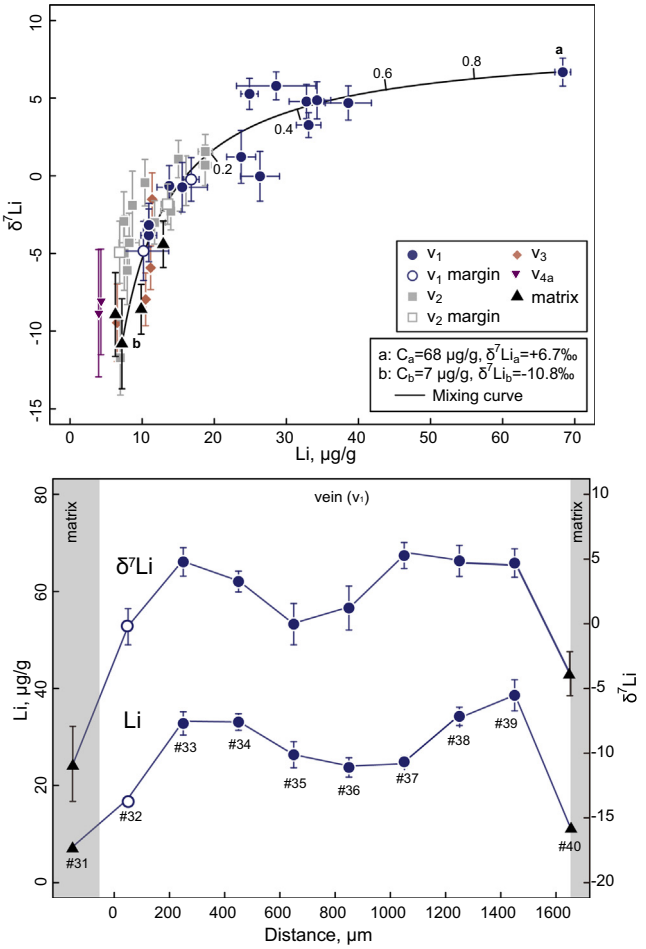

Fig. 8. (a) Li versus δ^7Li diagram for the New Idria jadeitite. Error bars represent a two-standard deviation of analytical reproducibility. Li concentration and δ^7Li within the sample varied widely ranging from 4 to 68 μg/g and from −11.7 to +6.7‰, respectively; these values show distributions along a curvilinear correlation regardless of the vein formation and occurrence. The black line represents a two end-member mixing model. The mixing equations are: $C = C_a \times f + C_b \times (1 - f)$ and $\delta^7Li = (\delta^7Li)_a \times f + (\delta^7Li)_b \times (1 - f)$, f = fraction of Li in end-member a (small letters). Li– δ^7Li variations within/among veins are due to variable mixing between initial infiltrating fluids (end-member a) and the matrix (end-member b). (b) Li concentration and δ^7Li for a traverse perpendicular to the v_1 walls. Note that symbols correspond to those in (a).

have δ^7Li values of +6.7 to +12.3‰. This value of the New Idria jadeitite-forming fluids indicates the high δ^7Li signatures of slab-derived fluids in a forearc mantle wedge. Marschall et al. (2007) modelled fluids released from average AOC at 50–300 °C range from $\delta^7Li = +21.5‰$ to +14.4‰. These compositions are much higher than the slab-derived fluids we inferred from the New Idria jadeitite in this study. Simons et al. (2010) also calculated the average subduction fluid with AOC plus GLOSS composition over 50–600 °C and found a fluid composition with $\delta^7Li = +7 \pm 5‰$ (1σ), which is consistent with jadeitite values in this study. For instance, the New Idria jadeitite, which are direct precipitates of slab-derived fluids, strongly supports the high δ^7Li signature of the slab-derived fluids and gives the values of $\delta^7Li = +6.7$ to +12.3‰ in a forearc mantle wedge.

Many studies have pointed out a dilemma that a high δ^7Li composition of slab-derived fluids is not consistent with δ^7Li composition in the primitive arcs basaltic rocks globally (+4.2 ± 1.6‰; Moriguti and Nakamura, 1998; Tomascak et al., 2000, 2002; Chan et al., 2002b). The New Idria jadeitite potentially provides a line of evidence for the presence of high δ^7Li fluids ($\delta^7Li = +6.7$ to +12.3‰) that dehydrated from a subducted slab and infiltrated into the mantle wedge at sub-forearc depth. Therefore, based on Rayleigh dehydration model, lower δ^7Li fluids should be dehydrated from a subducting slab at deeper sub-arc levels due to the progressive evolution of δ^7Li composition in the residual slab materials. The New Idria jadeitite also shows that high δ^7Li fluids were likely affected by interactions with the host matrix with a negative δ^7Li composition. This suggests that the signature of slab-derived fluids is easily modified by interactions with the surrounding rocks along their pathways, despite focused fluid flow in which fluids are not considered to be chemically affected by surrounding rocks. Therefore, the original signature of any slab-derived fluids may not be able to reach the regions of arc magma genesis in the core of the mantle wedge through fluid flow in the oceanic crust, sediment layer, mélange zone, and mantle wedge.

6. Perspectives: application of *in-situ*, spot Li isotopic analysis to H*P* rocks

The results of this study demonstrate the advantage of the *in-situ*, high-spatial resolution Li isotopic analyses developed by Kimura et al. (2016). Using this technique, we obtained the millimeter- to submillimeter-scale isotopic variations (~20‰) in a thin-section scale without the complexities of secondary whole rock modification. This application is useful for geochemical investigation of fluid–rock interaction in subduction zone; the record of the interaction is visible as H*P* mineral veins and/or H*P* rocks with 'rind' (e.g., John et al., 2012; Penniston-Dorland et al., 2010; Scambelluri and Philippot, 2001; Taetz et al., 2016, 2018; Tsujimori, 1997). Future applications of *in-situ* microanalytical techniques to such rocks will likely result in the discovery of similar isotopic variations and provide us with greater insights into slab-derived fluids.

7. Conclusions

(i) Microstructures and chemical compositions of jadeitite veins from the New Idria serpentinite body, California suggest that the veins were chemically affected by components of the matrix as host rocks of the veins during syntaxial vein formation.

(ii) High δ^{18}O data (Sorensen et al., 2006) and high concentrations of LILEs (Cs and Li) and HFSEs (Ta, Nb, U, and Th) in the New Idria jadeitite imply that the jadeite-forming fluids were derived from metasedimentary rocks.

(iii) *In-situ* Li isotopic analyses of the New Idria jadeitite confirmed a wide variation of δ^7Li from −11.7 to +6.7‰ accompanied with the change of Li concentrations from 4 to 68 μg/g. Variations within/among veins can be successfully modelled as variable mixing between the matrix and initial infiltrating fluids.

(iv) The initial slab-derived fluids to form the New Idria jadeitite are estimated to have δ^7Li values ranging from +6.7 to +12.3‰ based on the values that are supposed to be unmodified by the interactions with the matrix. The New Idria jadeitite potentially gives evidence of the presence of high δ^7Li fluids dehydrated from subducted slab materials and infiltration of the fluids into the mantle wedge at a sub-forearc depth.

Supplementary data to this article can be found online at https://doi.org/10.1016/j.lithos.2018.08.015.

Acknowledgements

This research was supported by Center for Northeast Asian Studies, Tohoku University and Japan Agency for Marine-Earth Science and Technology (JAMSTEC) in part by grants from the MEXT/JSPS KAKENHI JP15H05212 and JP18H01299 to T. Tsujimori and JP15H02148, JP16H01123 and JP18H04372 to J.-I. Kimura. This field work was supported in part by the International Joint Graduate Program in Earth

and Environmental Sciences (GP-EES) of Tohoku University. We are grateful for constructive reviews from R. Halama and K.E. Flores. We extend our appreciation to K. Aoki for his assistance on the EPMA analyses. We also thank Daniel Pastor-Galán for feedback.

References

Adam, J., Locmelis, M., Afonso, J.C., Rushmer, T., Fiorentini, M.L., 2014. The capacity of hydrous fluids to transport and fractionate incompatible elements and metals within the Earth's mantle. Geochemistry Geophysics Geosystems 15, 2241–2253.

Atwater, B.F., Trumm, D.A., Tinsley III, J.C., Stein, R.S., Tucker, A.B., Donahue, D.J., Jull, A.J.T., Payen, L.A., 1990. Alluvial Plains and Earthquake Recurrence at the Coalinga Anticline. United States Geological Survey Professional Paper 1487. p. 273.

Blundy, J., Wood, B., 1994. Prediction of crystal–melt partition coefficients from elastic moduli. Nature 372 (6505), 452.

Bons, P.D., Elburg, M.A., Gomez-Rivas, E., 2012. A review of the formation of tectonic veins and their microstructures. Journal of Structural Geology 43, 33–62.

Bouman, C., Elliott, T., Vroon, P.Z., 2004. Lithium inputs to subduction zones. Chemical Geology 212, 59–79.

Brenan, J.M., Ryerson, F.J., Shaw, H.F., 1998. The role of aqueous fluids in the slab-to-mantle transfer of boron, beryllium, and lithium during subduction: Experiments and models. Geochimica et Cosmochimica Acta 62, 3337–3347.

Chan, L.H., Edmond, J.M., Thompson, G., Gillis, K., 1992. Lithium isotopic composition of submarine basalts: implications for the lithium cycle in the oceans. Earth and Planetary Science Letters 108 (1–3), 151–160.

Chan, L.H., Alt, J.C., Teagle, D.A.H., 2002a. Lithium and lithium isotope profiles through the upper oceanic crust: a study of seawater–basalt exchange at ODP Sites 504B and 896A. Earth and Planetary Science Letters 201, 187–201.

Chan, L.H., Leeman, W.P., You, C.F., 2002b. Lithium isotopic composition of Central American volcanic arc lavas: Implications for modification of subarc mantle by slab-derived fluids: Correction. Chemical Geology 182, 293–300.

Chan, L.H., Leeman, W.P., Plank, T., 2006. Lithium isotopic composition of marine sediments. Geochemistry, Geophysics, Geosystems 7 (6).

Coleman, R.G., 1961. Jadeite deposits of the Clear Creek area, New Idria district, San Benito County, California. Journal of Petrology 2 (2), 209–247.

Coleman, R.G., 1986. Ophiolites and accretion of the North American Cordillera. Bulletin de la Socité Géologique de France 2, 961–968.

Coogan, L.A., Kasemann, S.A., Chakraborty, S., 2005. Rates of hydrothermal cooling of new oceanic upper crust derived from lithium-geospeedometry. Earth and Planetary Science Letters 240, 415–424.

Cowan, D.S., Mansfield, C.F., 1970. Serpentinite flows on Joa- quin Ridge, southern coast ranges, California. Geological Society of America Bulletin 81, 2615–2628.

Flores, K.E., Martens, U.C., Harlow, G.E., Brueckner, H.K., Pearson, N.J., 2013. Jadeitite formed during subduction: In situ zircon geochronology constraints from two different tectonic events within the Guatemala Suture Zone. Earth and Planetary Science Letters 371, 67–81.

Kayama, M., Nishido, H., Toyoda, S., Komuro, K., Ninagawa, K., 2011. Combined cathodoluminescence and micro–Raman study of helium–ion–implanted albite. Spectroscopy Letters 44, 526–529.

Kimura, J.-I., Chang, Q., 2012. Origin of the suppressed matrix effect for improved analytical performance in determination of major and trace elements in anhydrous silicate samples using 200 nm femtosecond laser ablation sector-field inductively coupled plasma mass spectrometry. Journal of Analytical Atomic Spectrometry 27 (9), 1549–1559.

Kimura, J.-I., Gill, J.B., Kunikiyo, T., Osaka, I., Shimoshioiri, Y., Katakuse, M., Kakubuchi, S., Nagao, T., Furuyama, K., Kamei, A., Kawabata, H., Nakajima, J., van Keken, P.E., Stern, R.J., 2014. Diverse magmatic effects of subducting a hot slab in SW Japan: Results from forward modeling. Geochemistry Geophysics Geosystems 15, 691–739.

Kimura, J.-I., Chang, Q., Ishikawa, T., Tsujimori, T., 2016. Influence of laser parameters on isotope fractionation and optimisation of lithium and boron isotope ratio measurements using laser ablation-multiple Faraday collector-inductively coupled plasma mass spectrometry. Journal of Analytical Atomic Spectrometry 31 (11), 2305–2320.

Kimura, J.-I., 2017. Modeling chemical geodynamics of subduction zones using the Arc Basalt Simulator version 5. Geosphere 13, 992–1025.

Halama, R., John, T., Herms, P., Hauff, F., Schenk, V., 2011. A stable (Li, O) and radiogenic (Sr, Nd) isotope perspective on metasomatic processes in a subducting slab. Chemical Geology 281, 151–166.

Harlow, G.E., Tsujimori, T., Sorensen, S.S., 2015. Jadeitites and Plate Tectonics. Annual Review of Earth and Planetary Sciences 43, 105–138.

Hermann, J., Spandler, C., 2008. Sediment melts at sub-arc depths: an experimental study. Journal of Petrology 49 (4), 717–740.

James, R.H., Palmer, M.R., 2000. The lithium isotope composition of international rock standards. Chemical Geology 166 (3–4), 319–326.

John, T., Klemd, R., Klemme, S., Pfänder, J.A., Hoffmann, J.E., Gao, J., 2011. Nb–Ta fractionation by partial melting at the titanite–rutile transition. Contributions to Mineralogy and Petrology 161 (1), 35–45.

John, T., Gussone, N., Podladchikov, Y.Y., Bebout, G.E., Dohmen, R., Halama, R., Klemd, R., Mgna, T., Seitz, H.M., 2012. Volcanic arcs fed by rapid pulsed fluid flow through subducting slabs. Nature Geoscience 5, 489–492.

Marks, M., Halama, R., Wenzel, T., Markl, G., 2004. Trace element variations in clinopyroxene and amphibole from alkaline to peralkaline syenites and granites: implications for mineral–melt trace-element partitioning. Chemical Geology 211 (3), 185–215.

Marschall, H.R., Pogge Von Strandmann, P.A.E., Seitz, H.M., Elliott, T., Niu, Y., 2007. The lithium isotopic composition of orogenic eclogites and deep subducted slabs. Earth and Planetary Science Letters 262, 563–580.

Maruyama, S., Liou, J.G., 1988. Petrology of Franciscan metabasites along the jadeite-glaucophane type facies series. Cazadero, California, Journal of Petrology 29 (1), 1–37.

McDonough, W.F., Sun, S.S., 1995. The composition of the Earth. Chemical Geology 120 (3–4), 223–253.

Millot, R., Scaillet, B., Sanjuan, B., 2010. Lithium isotopes in island arc geothermal systems: Guadeloupe, Martinique (French West Indies) and experimental approach. Geochimica et Cosmochimica Acta 74 (6), 1852–1871.

Moriguti, T., Nakamura, E., 1998. Across-arc variation of Li isotopes in lavas and implications for crust/mantle recycling at subduction zones. Earth and Planetary Science Letters 163 (1), 167–174.

Okamoto, A., Sekine, K., 2011. Textures of syntaxial quartz veins synthesized by hydrothermal experiments. Journal of Structural Geology 33 (12), 1764–1775.

Penniston-Dorland, S.C., Sorensen, S.S., Ash, R.D., Khadke, S.V., 2010. Lithium isotopes as a tracer of fluids in a subduction zone mélange: Franciscan Complex, CA. Earth and Planetary Science Letters 292, 181–190.

Penniston-Dorland, S.C., Bebout, G.E., von Strandmann, P.A.P., Elliott, T., Sorensen, S.S., 2012. Lithium and its isotopes as tracers of subduction zone fluids and metasomatic processes: Evidence from the Catalina Schist, California, USA. Geochimica et Cosmochimica Acta 77, 530–545.

Plank, T., Langmuir, C.H., 1998. The chemical composition of subducting sediment and its consequences for the crust and mantle. Chemical Geology 145, 325–394.

Ramsay, J.G., 1980. The crack–seal mechanism of rock deformation. Nature 284 (5752), 135.

Richter, F.M., Liang, Y., Davis, A.M., 1999. Isotope fractionation by diffusion in molten oxides. Geochimica et Cosmochimica Acta 63 (18), 2853–2861.

Richter, F.M., Davis, A.M., Depaolo, D.J., Watson, E.B., 2003. Isotope fractionation by chemical diffusion between molten basalt and rhyolite. Geochimica et Cosmochimica Acta 67 (20), 3905–3923.

Scambelluri, M., Philippot, P., 2001. Deep fluids in subduction zones. Lithos 55 (1–4), 213–227.

Simons, K.K., Harlow, G.E., Brueckner, H.K., Goldstein, S.L., Sorensen, S.S., Hemming, N.G., Langmuir, C.H., 2010. Lithium isotopes in Guatemalan and Franciscan HP-LT rocks: Insights into the role of sediment-derived fluids during subduction. Geochimica et Cosmochimica Acta 74, 3621–3641.

Sorensen, S., Harlow, G.E., Rumble, D., 2006. The origin of jadeitite-forming subduction-zone fluids: CL-guided SIMS oxygen-isotope and trace-element evidence. American Mineralogist 91, 979–996.

Staudigel, H., Plank, T., White, B., Schmincke, H.U., 1996. Geochemical fluxes during seafloor alteration of the basaltic upper oceanic crust: DSDP Sites 417 and 418. Subduction: Top to Bottom 96, pp. 19–38.

Taetz, S., John, T., Bröcker, M., Spandler, C., 2016. Fluid–rock interaction and evolution of a high-pressure/low-temperature vein system in eclogite from New Caledonia: insights into intraslab fluid flow processes. Contributions to Mineralogy and Petrology 171, 90.

Taetz, S., John, T., Bröcker, M., Spandler, C., Stracke, A., 2018. Fast intraslab fluid-flow events linked to pulses of high pore fluid pressure at the subducted plate interface. Earth and Planetary Science Letters 482, 33–43.

Takahashi, N., Tsujimori, T., Kayama, M., Nishido, H., 2017. Cathodoluminescence petrography of P–type jadeitites from the New Idria serpentinite body, California. Journal of Mineralogical and Petrological Sciences 112 (5), 291–299.

Tatsumi, Y., Eggins, S., 1995. Subduction zone magmatism 1. Wiley.

Teng, F.Z., McDonough, W.F., Rudnick, R.L., Walker, R.J., 2006. Diffusion-driven extreme lithium isotopic fractionation in country rocks of the Tin Mountain pegmatite. Earth and Planetary Science Letters 243, 701–710.

Tomascak, P.B., Ryan, J.G., Defant, M.J., 2000. Lithium isotope evidence for light element decoupling in the Panama subarc mantle. Geology 28 (6), 507–510.

Tomascak, P.B., Widom, E., Benton, L.D., Goldstein, S.L., Ryan, J.G., 2002. The control of lithium budgets in island arcs. Earth and Planetary Science Letters 196, 227–238.

Tomascak, P.B., Langmuir, C.H., le Roux, P.J., Shirey, S.B., 2008. Lithium isotopes in global mid-ocean ridge basalts. Geochimica et Cosmochimica Acta 72 (6), 1626–1637.

Tsujimori, T., 1997. Omphacite-diopside vein in an omphacitite block from the Osayama serpentinite melange, Sangun-Renge metamorphic belt, southwestern Japan. Mineralogical Magazine 61, 845–852.

Tsujimori, T., Liou, J.G., Coleman, R.G., 2005. Coexisting retrograde jadeite and omphacite in a jadeite-bearing lawsonite eclogite from the Motagua Fault Zone, Guatemala. American Mineralogist 90 (5–6), 836–842.

Tsujimori, T., Liou, J.G., Coleman, R.G., 2007. Finding of high–grade tectonic blocks from the New Idria serpentinite body, Diablo Range, California: Petrologic constraints on the tectonic evolution of an active serpentinite diapir. Geological Society of America Special Papers 419, 67–80.

Tsujimori, T., Harlow, G.E., 2012. Petrogenetic relationships between jadeitite and associated high-pressure and low-temperature metamorphic rocks in worldwide jadeitite localities: a review. European Journal of Mineralogy 24 (2), 371–390.

Tsujimori, T., Harlow, G.E., 2017. Jadeitite (jadeite jade) from Japan: History, characteristics, and perspectives. Journal of Mineralogical and Petrological Sciences 112 (5), 184–196.

Wang, Y., Merino, E., 1992. Dynamic model of oscillatory zoning of trace elements in calcite: Double layer, inhibition, and self-organization. Geochimica et Cosmochimica Acta 56, 581–596.

Wunder, B., Meixner, A., Romer, R.L., Heinrich, W., 2006. Temperature-dependent isotopic fractionation of lithium between clinopyroxene and high-pressure hydrous fluids. Contributions to Mineralogy and Petrology 151, 112–120.

Wunder, B., Meixner, A., Romer, R.L., Feenstra, A., Schettler, G., Heinrich, W., 2007. Lithium isotope fractionation between Li-bearing staurolite, Li-mica and aqueous fluids: An experimental study. Chemical Geology 238, 277–290.

Yang, D., Hou, Z., Zhao, Y., Hou, K., Yang, Z., Tian, S., Fu, Q., 2015. Lithium isotope traces magmatic fluid in a seafloor hydrothermal system. Scientific Reports 5, 13812.

Zack, T., Tomascak, P.B., Rudnick, R.L., Dalpé, C., McDonough, W.F., 2003. Extremely light Li in orogenic eclogites: The role of isotope fractionation during dehydration in subducted oceanic crust. Earth and Planetary Science Letters 208, 279–290.